Chaotic scattering and the magneto-Coulomb map

B. Hu,[1] W. Horton,[1] and T. Petrosky[2,3]
[1]*Institute for Fusion Studies, The University of Texas, Austin, Texas 78712*
[2]*Center for Studies in Statistical Mechanics and Complex Systems, The University of Texas, Austin, Texas 78712*
[3]*International Solvay Institutes for Physics and Chemistry, CP231, 1050 Brussels, Belgium*
(Received 23 January 2002; published 13 May 2002)

A nonrelativistic classical electron scattering by a fixed ion in a uniform magnetic field is discussed. The system is nonintegrable, and there is chaotic scattering for a certain class of initial conditions. A two-dimensional discrete map is derived from the equation of motion. Our map exhibits four different types of motion by changing the parameters which characterize the initial condition. The fractal structure for certain observables is obtained. The width of the chaotic scattering region in the impact parameter is estimated numerically. We suggest a certain class of plasma environments where the chaotic scattering may have an important role.

DOI: 10.1103/PhysRevE.65.056212 PACS number(s): 05.45.−a

I. INTRODUCTION

In this paper, we consider the problem of a nonrelativistic classical electron scattering by a fixed ion in a uniform magnetic field. This system is nonintegrable, hence one can expect the appearance of the chaotic scattering for certain class of initial conditions. Indeed, this has been noticed by Delos *et al.* [1] and analyzed later by Schmidt *et al.* [2] (also see [3–8] for the trapped motion of the electron in the classical case as well as in the quantum case). So far, all analyses were based on the continuous flow generated by the equation of motion. However, as we shall show below, that there are many cyclotron periods in a single scattering during the electron-ion interaction time interval. As a result, the numerical integration of the equation of motion for the continuous flow is very time consuming and the predictions for long-time behavior become unstable, which is the typical case of the chaotic scattering. For this reason, we shall derive a discrete map of the chaotic scattering.

In order to get a picture of the chaotic scattering, let us first consider the case that an incoming electron with an initial velocity parallel to the magnetic field in the z direction (see Fig. 1). We will consider more general initial conditions later. Suppose the electron is scattered by a nearly 90° angle, and it starts doing cyclotron motion in the neighborhood of the ion. Due to the attractive force from the ion, while doing circular motion in the xy plane, the electron oscillates along the z direction, and eventually escapes in the forward or backward direction. In the phase space, there is a domain where the scattered electron is very sensitive with respect to a slight change of the initial condition. In Fig. 1, the two-electron orbits have been numerically integrated from the equation of motion (10) given later. Both of the electrons have the same dimensionless initial velocity $\boldsymbol{v}(t=0)=1.0\hat{\boldsymbol{z}}$ and the dimensionless position $z(t=0)$, but with a slightly different dimensionless impact parameters, i.e., $b=1.02$ and $b=1.03$, respectively. The normalization will be introduced in Sec. II. Eventually, the electron in Fig. 1(a) is scattered backward, while the electron in Fig. 1(b) is scattered forward. These examples show that, indeed, many cyclotron periods appear before the oscillation in the z direction ends.

The structure of this paper is as follows: In Sec. II, we shall derive a two-dimensional map for the position z and the velocity v_z in the z direction, where the position is taken to be the farthest point from the ion in each cyclotron period. The derivation of the map which works for the general situation is a difficult task due to the nonintegrability. Hence, in this paper, we restrict our interest to a case where the influence of the Coulomb force may be considered as a small perturbation over the cyclotron motion. This situation can be achieved for the case where the electron has a large velocity in the cyclotron motion. As we shall see, we can derive a desirable map with a relatively simple calculation for this case.

In Sec. III, the comparison of our map with the numerical integration is presented. As we shall see, the agreement is excellent.

In Sec. IV, we shall display the phase plots obtained from our map for several situations, including trapped motion near the chaotic scattering regime and the case for the chaotic scattering. Our map shows that there exist islands that correspond to the trapped motion inside the chaotic scattering region.

In Sec. V, we shall discuss a parameter d dependence of motion, where d is defined as the distance of the guiding center line of the electron orbit from the ion. Our map shows that there appear four different types of motion, depending on d. These different motions appear by changing d from small value to large value, in such a way that for small value we have a trapped chaotic orbit, then chaotic scattering orbit, again trapped chaotic orbit, and finally for large d we obtain a regular scattering orbit. We shall analytically explain the origin of these four different types of motion.

In Sec. VI, we shall display the fractal structure in the final velocity v_z^f in the z direction and the bouncing number n_z of orbit before the electron escapes to infinity.

In Sec. VII, we shall numerically analyze the width of the chaotic scattering region in the impact parameter as a

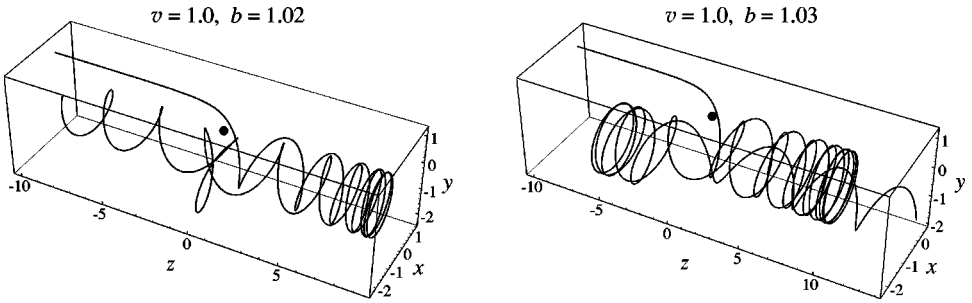

FIG. 1. Initial sensitivity for chaotic scattering is shown in terms of the two electron orbits. The dot denotes the ion. Initial conditions are (a) $b=1.02$ and (b) $b=1.03$ with the same $z(t=0)=-10$ and $\boldsymbol{v}(t=0)=1.0\hat{\boldsymbol{z}}$.

function of the velocity v of the electron. We shall see that the smaller the velocity v, the wider the chaotic region.

In the last section, we shall give a comment on the plasma environment, where the chaotic scattering may play an important role.

II. DERIVATION OF MAP

We consider an electron in a Coulomb potential of a fixed ion with a charge Ze at the origin together with a uniform magnetic field $\boldsymbol{B}=B\hat{\boldsymbol{z}}$. The Hamiltonian in the cylindrical coordinates $(\tilde{r},\tilde{\phi},\tilde{z})$ and the momenta $(\tilde{P}_r,\tilde{P}_\phi,\tilde{P}_z)$ is

$$\tilde{H}=\frac{\tilde{P}_r^2}{2m_e}+\frac{\tilde{P}_z^2}{2m_e}+\frac{1}{2m_e}\left(\frac{\tilde{P}_\phi}{\tilde{r}}+\frac{\omega_c m_e\tilde{r}}{2}\right)^2-\frac{1}{4\pi\epsilon_0}\frac{Ze^2}{\sqrt{\tilde{r}^2+\tilde{z}^2}}, \tag{1}$$

where the variables with dimensions are denoted by the tildes. There is a characteristic time scale, i.e., the cyclotron frequency

$$\omega_c=\frac{eB}{m_e}, \tag{2}$$

which can be used to introduce the dimensionless time t,

$$t=\omega_c\tilde{t}. \tag{3}$$

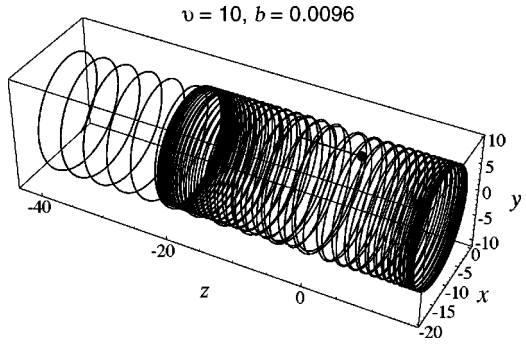

FIG. 2. A typical orbit of the chaotic scattering. The dot denotes the ion. The electron starts from the left to the ion ($z=-10$) with a velocity $v=10$ in the z direction, and an impact parameter $b=0.0096$. After the electron is scattered by a nearly 90° angle, the guiding center is moving in a nearly straight line parallel to the magnetic field, and the electron is doing a nearly circular motion in the xy plane.

A space scale r_0 is defined as the radius of a circular Keplerian motion such that the Keplerian frequency is equal to the cyclotron frequency

$$\frac{1}{r_0^{3/2}}\sqrt{\frac{Ze^2}{4\pi\epsilon_0 m_e}}=\omega_c, \quad r_0=\left(\frac{Zm_e}{4\pi\epsilon_0 B^2}\right)^{1/3}, \tag{4}$$

and the length is normalized as

$$\boldsymbol{r}=\tilde{\boldsymbol{r}}/r_0. \tag{5}$$

In this system, there are two invariants of motion, i.e., the energy and the angular momentum. These invariants are also normalized as

$$P_\phi=\frac{\tilde{P}_\phi}{m_e\omega_c^2 r_0}, \quad \mathcal{E}=\frac{\tilde{\mathcal{E}}}{m_e\omega_c^2 r_0^2}. \tag{6}$$

We have

$$P_\phi=(x\dot{y}-y\dot{x})-\frac{1}{2}(x^2+y^2), \tag{7}$$

$$\mathcal{E}=\frac{1}{2}(\dot{x}^2+\dot{y}^2+\dot{z}^2)-\frac{1}{(x^2+y^2+z^2)^{1/2}}. \tag{8}$$

The dimensionless Hamiltonian is given by

$$H=\frac{P_r^2}{2}+\frac{P_z^2}{2}+\frac{1}{2}\left(\frac{P_\phi}{r}+\frac{r}{2}\right)^2-\frac{1}{\sqrt{r^2+z^2}}. \tag{9}$$

This leads to the equation of motion

$$\ddot{\boldsymbol{r}}=\dot{\boldsymbol{r}}\times\hat{\boldsymbol{z}}-\frac{\hat{\boldsymbol{r}}}{r^2}. \tag{10}$$

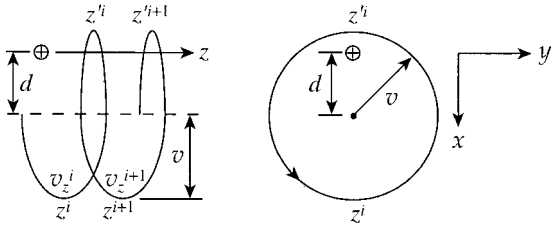

FIG. 3. Variables in the map.

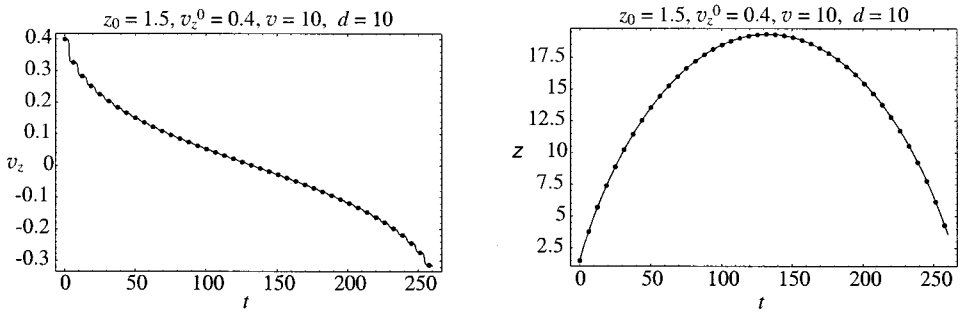

FIG. 4. The comparison between the map and the numerical integration for (z,v_z) vs t. The initial condition is $z^0=1.5$, $v_z^0=0.4$, $v=10$, and $d=10$. The cyclotron period is 2π.

There is no parameter in the equation of motion, hence the only controllable factor is the initial condition in the dimensionless units. We note that the equation of motion (10) has a similar structure for the restricted three-body problem in celestial mechanics where the Coriolis force corresponds to the magnetic force [6,9]. For this case the chaotic scattering in the vicinity of the parabolic motion has been noticed [10].

For the scattering problem, both the incoming and the outgoing states of the electron are generally helical cyclotron orbits (see, e.g., Fig. 9). In order to get a map in a simple form that exhibits a chaotic behavior, we restrict our interest to the case where the Coulomb force may be treated as a small perturbation to the magnetic force. One can easily expect that this can be achieved if the two conditions

$$v_z \ll v \quad \text{and} \quad v \gg 1, \tag{11}$$

are satisfied during the cyclotron motion, where v_z is the component of $\boldsymbol{v}$ parallel to z. Indeed, the first condition $v_z \ll v$ gives $v_\perp \approx v$, where $v_\perp$ is the component of $\boldsymbol{v}$ perpendicular to z. This condition gives the dimensionless cyclotron radius $\rho_e \approx v$. Due to the second condition $v \gg 1$, the electron spends almost all the time far from the ion, and the cyclotron motion dominates during each cyclotron period. Thus, the Coulomb force may be treated as a small perturbation. Then again due to the first condition of Eq. (11), the motion of the guiding center of the electron is so slow that the Coulomb force may give a long-time resonance effect that leads to a chaotic motion.

Moreover, one may expect that if the condition (11) is satisfied, the distance between the guiding center line and the ion remains nearly constant during the scattering for almost all initial conditions. Indeed the numerical integration has verified this prediction. In Fig. 2, we show a typical orbit of the chaotic scattering that satisfies the condition (11). We see that the motion in the xy plane is nearly circular and the guiding center is moving in a nearly straight line parallel to the magnetic field.

Under this consideration we now construct the map as follows. Let d be the distance between the ion and the guiding center line. In Fig. 3, we illustrate a configuration for the construction of the map. In this figure, v_z^i and z^i are defined as the z and v_z at the farthest points of the electron from the ion in the xy plane, and z'^i is defined as the z at the closest points of the electron from the ion in the xy plane for each cyclotron motion. First we construct an auxiliary map for the variable pair (v_z^i, z'^i). From the equation of motion the change in v_z at the farthest point to the ion during one cyclotron motion is evaluated as

$$v_z^{i+1} - v_z^i \approx \int_0^{2\pi} \frac{z(t)dt}{[z(t)^2 + v^2 + d^2 - 2vd\cos t]^{3/2}}, \tag{12}$$

where we have approximated that the cyclotron radius $\rho_e(t) \approx v$ and $d(t) \approx d$ with given constants v and d, and approximated that the electron does a uniform circular motion of period 2π. Moreover, because of the condition (11) of the small perturbation during each cyclotron period, we may approximate $z(t)$ by a constant z'^i. Then we have

$$v_z^{i+1} - v_z^i \approx \int_0^{2\pi} \frac{z'^i dt}{[z'^{i2} + v^2 + d^2 - 2vd\cos t]^{3/2}} = \frac{4z'^i\sqrt{(d-v)^2 + z'^{i2}}}{(d^2 - v^2 + z'^{i2})^2 + 4v^2 z'^{i2}} E\left[\frac{-4dv}{(d-v)^2 + z'^{i2}}\right], \tag{13}$$

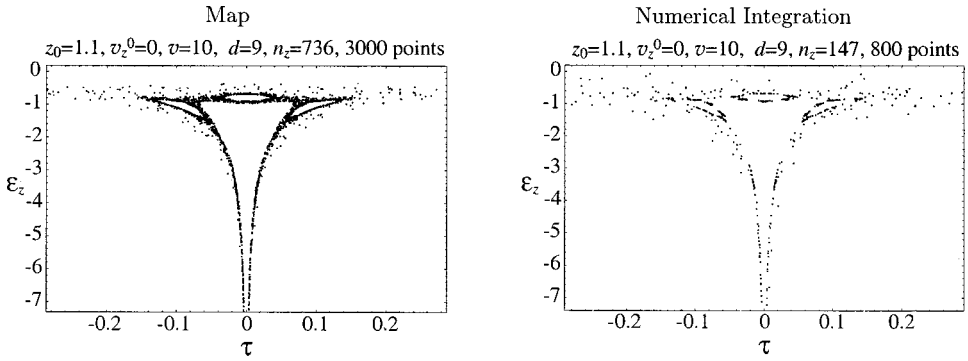

FIG. 5. The comparison of the phase-space (ε_z, τ) plots between the map and the numerical integration for the trapped chaotic motion near scattering regime. The initial condition is $z^0=1.1$, $v_z^0=0$, $v=10$, and $d=9$.

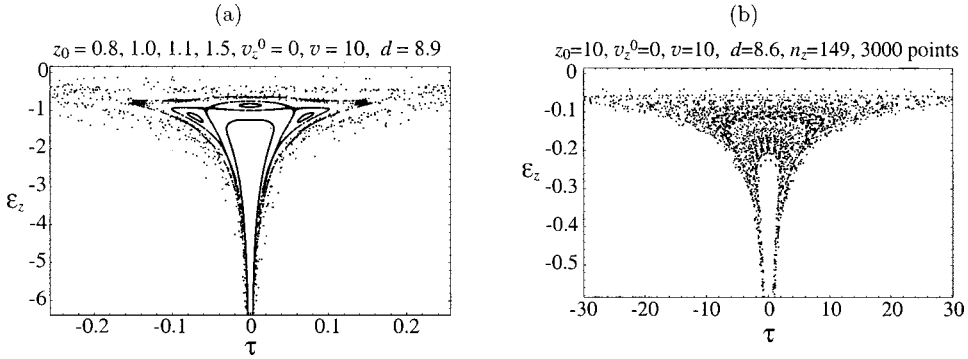

FIG. 6. Trapped chaotic motion near scattering regime in phase-space (ε_z,τ) plots.

where $E(m)$ is the complete elliptic integral of the second kind.

To estimate the change in z', we further approximate that the electron has a constant velocity $v_z \approx v_z^{i+1}$ between z'^i and z'^{i+1}. Then we have

$$z'^{i+1}-z'^{i}=2\pi v_z^{i+1}. \tag{14}$$

A set of Eqs. (13) and (14) gives a two-dimensional area-preserving map. In this map, the two variables (v_z^i,z'^i) are defined at different points, i.e., the aphelion for v_z^i and the perihelion for z'^i, respectively.

In order to have a map with two variables defined at the same point, e.g., the aphelion, we use the pair (v_z^i,z^i) and approximate as

$$z^i=z'^i-\pi v_z^i. \tag{15}$$

Then we obtain a final form of the map for (v_z^i,z^i), which is also area preserving,

$$\begin{aligned} v_z^{i+1}&=v_z^i+\frac{4(z^i+\pi v_z^i)\sqrt{(d-v)^2+(z^i+\pi v_z^i)^2}}{[d^2-v^2+(z^i+\pi v_z^i)^2]^2+4v^2(z^i+\pi v_z^i)^2}\\ &\quad\times E\left[\frac{-4dv}{(d-v)^2+(z^i+\pi v_z^i)^2}\right],\\ z^{i+1}&=z^i+\pi(v_z^i+v_z^{i+1}). \end{aligned} \tag{16}$$

We call this map the ''magneto-Coulomb map.''

In order to have a criterion for the electron to escape without being bounced back in the z direction, it is convenient to write the map in terms of the Keplerian energy ε_z and its canonical conjugate τ defined by

$$\begin{aligned} \varepsilon_z&=\frac{1}{2}v_z^2-\frac{1}{|z|},\\ \tau&=\mathrm{sgn}(z)\left(\frac{v_z}{\varepsilon_z(-2\varepsilon_z+v_z^2)}-\frac{1}{\sqrt{2}|\varepsilon_z|^{3/2}}\tan^{-1}\frac{v_z}{\sqrt{2|\varepsilon_z|}}\right). \end{aligned} \tag{17}$$

The derivation of τ will be presented at the end of this section. The comparison of the chaotic scattering with the case in which the electron moves in a straight line along the z axis without the magnetic field with the same initial values v_z^0 and z^0 shows that, if the latter electron can escape, i.e., $\varepsilon_z^0=\frac{1}{2}(v_z^0)^2-1/|z^0|>0$, then the former one can also escape. Then the electron escape criterion is

$$\varepsilon_z\geqslant 0 \quad \text{and} \quad zv_z\geqslant 0. \tag{18}$$

Here we have introduced the second condition for the sign of zv_z, to ensure that the electron is leaving the ion and will never come back.

The variable τ is calculated from the equation of motion for the one-dimensional Kepler problem without the magnetic field,

$$\frac{dv_z}{d\tau}=-\mathrm{sgn}(z)\frac{1}{z^2}, \tag{19}$$

and the relation $\varepsilon_z=\frac{1}{2}v_z^2-1/|z|$. We have

$$\begin{aligned} \tau&=-\mathrm{sgn}(z)\int^{v_z}dv_z\left(\frac{1}{2}v_z^2-\varepsilon_z\right)^{-2}\\ &=\mathrm{sgn}(z)\left(\frac{v_z}{\varepsilon_z(-2\varepsilon_z+v_z^2)}-\frac{1}{\sqrt{2}|\varepsilon_z|^{3/2}}\tan^{-1}\frac{v_z}{\sqrt{2|\varepsilon_z|}}\right)+C. \end{aligned} \tag{20}$$

The integration constant $C=0$ is determined by imposing the condition that τ is continuous at $z=0$ where $\varepsilon_z\to-\infty$. We note that Eq. (20) ensures area preserving

$$\frac{\partial(\varepsilon_z,\tau)}{\partial(v_z,z)}=1. \tag{21}$$

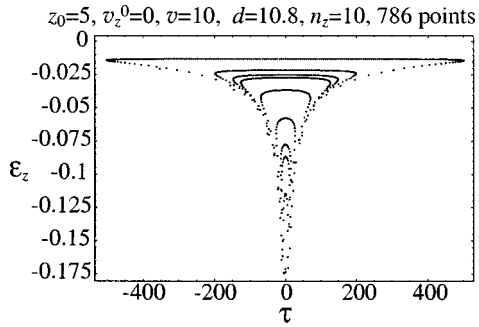

FIG. 7. Phase-space plot for scattering motion.

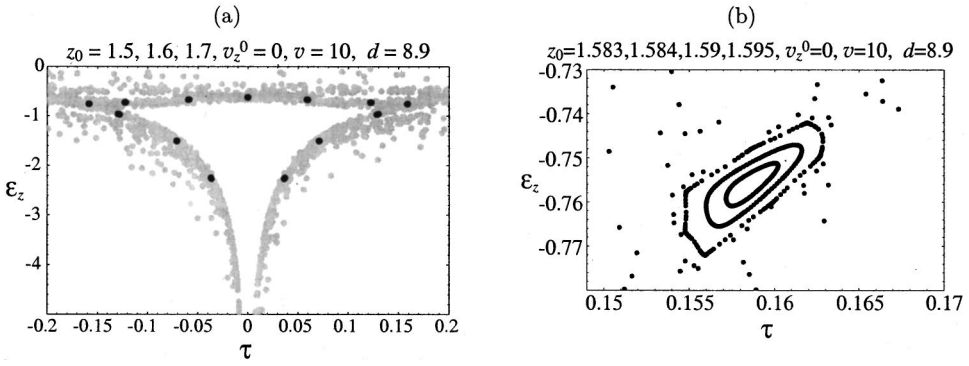

FIG. 8. Islands of the trapped motion inside the scattering region.

III. COMPARISON OF MAP WITH NUMERICAL INTEGRATION

In order to see the accuracy of our map, we compare the results from the map to those from the numerical integration. Because of the choice of the coordinate system in Fig. 3, the initial condition (z^0, v_z^0) and the parameters (v, d) in the map correspond to $x = v + d$, $y = 0$, $v_x = 0$, $v_y = v$, $z = z^0$, and $v_z = v_z^0$ in the numerical integration. The numerical integration has been performed by MATHEMATICA with the Gauss-Kronrod method.

In Fig. 4, we show the comparison between the map and the numerical integration for the time evolution of $\{z(t), v_z(t)\}$ with $z^0 = 1.5$, $v_z^0 = 0.4$, $v = 10$, and $d = 10$, where the lines denote the results from the numerical integration and the dots denote the results from the map. The agreement between the map and the numerical integration is excellent.

In Fig. 5, we show the comparison between the map and the numerical integration in the phase-space (ε_z, τ) plot for the initial condition: $z^0 = 1.1$, $v_z^0 = 0$, $v = 10$, and $d = 9$. From the map (17), we see that $\varepsilon_z \to -\infty$ as $\tau \to 0$ (that corresponds to $z \to 0$). In Fig. 5, the points corresponding to large $|\varepsilon_z|$ are not shown.

For the individual trajectory there is a slight difference between the map and the numerical integration. However, the ensemble of the points has essentially the same structure (e.g., the location of the islands and the chaotic region), which is a well-known feature of the phase-space plots in the chaotic dynamics that are generated from the different algorithms.

IV. PHASE-SPACE PLOTS

In this section, we shall show the phase-space plots (ε_z, τ) that have been created from the map for several situations of the trapped motion and of the scattering motion.

In Fig. 6, we have plotted the trapped motion near the scattering regime. Figure 6(a) has been created from four initial conditions: $z^0 = 0.8, 1.0, 1.1$, and 1.5 with the same $v_z^0 = 0$, $v = 10$, and $d = 8.9$. For the chaotic motion, we have plotted up to 1000 iterations. Figure 6(b) is also the trapped motion, but is much closer to the scattering regime than the ones in Fig. 6(a). The figure has been created from a single

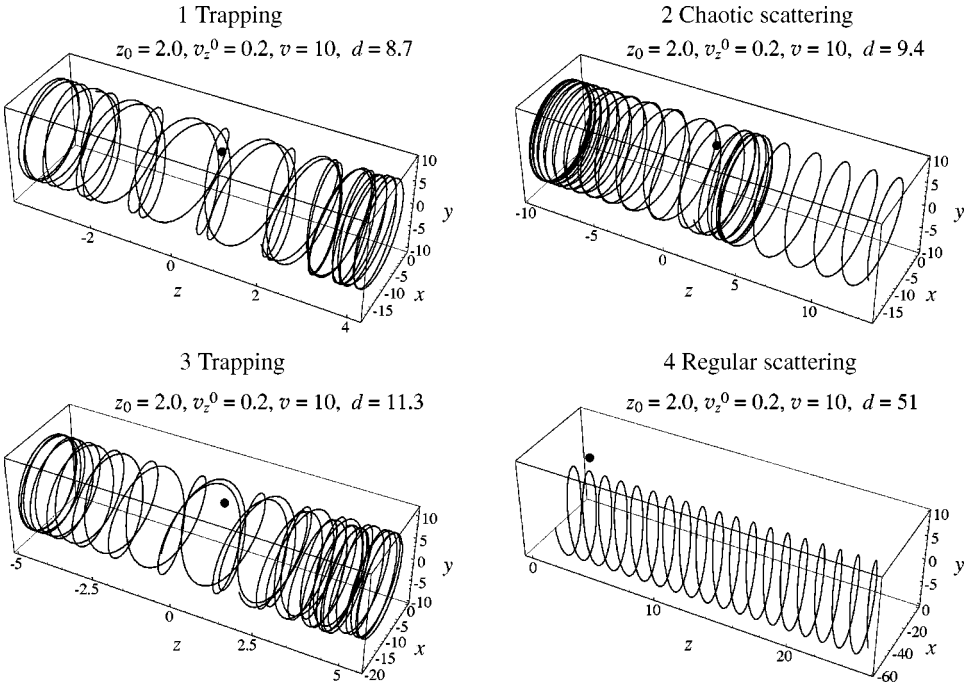

FIG. 9. Four types of orbits, i.e., 1 trapping, 2 chaotic scattering, 3 trapping, and 4 regular scattering. The initial condition $z^0 = 2.0$, $v_z^0 = 0.2$, and the parameter $v = 10$ are the same for all the four cases, but the parameter d is different, i.e., $d = 8.7$, 9.4, 11.3, and 51, respectively.

initial condition, $z^0=10$, $v_z^0=0$, $v=10$, and $d=8.6$. Note that the domain of τ is much larger and ε_z is more closer to zero than the ones in Fig. 6(a).

In Fig. 7, we have plotted a scattering motion. The initial condition is $z^0=5$, $v_z^0=0$, $v=10$, and $d=10.8$. After 768 cyclotron periods, we have $\varepsilon_z>0$ and the electron has escaped toward the infinity from the ion. When the electron passes the ion each time, the point jumps randomly from one loop to another, and it eventually escapes. We notice the large size of the figure in τ direction, and smaller value of $|\varepsilon_z|$.

In Fig. 8, we show the islands of the trapped orbits inside the chaotic scattering region. In Fig. 8(a), the gray points are the scattered orbits generated from two initial conditions: $z^0=1.5$ and 1.7, with the same $v_z^0=0$, $v=10$, and $d=8.9$. These points have escaped to $\varepsilon_z>0$ after 7835 and 2091 cyclotron periods, respectively. The dark points in Fig. 8(a) are the periodical points of period 13, with the initial condition: $z^0=1.6$, $v_z^0=0$, $v=10$, and $d=8.9$. The magnified section of the right-most dark point is shown in Fig. 8(b). We see the island structure of the trapped motion. The points are generated from four different initial conditions: $z^0=1.583$, 1.584, 1.59, and 1.595, with the same $v_z^0=0$, $v=10$, and $d=8.9$. The case with $z^0=1.583$ gives the scattered orbit.

V. *D* DEPENDENCE OF MOTION

In this section, we consider a d dependence of the motion of the electron for a given v and with a given initial condition (z^0,v_z^0). By increasing d, we found four different types of motion. They are as follows:

(1) if $d\ll v$, the motion is trapped;
(2) if $d\sim v$, the motion is chaotic scattering;
(3) if $d\gg v$, the motion is trapped again; and
(4) if we increase d further, we then have nonchaotic scattering motion.

In Fig. 9, we show the four corresponding orbits that are generated from the numerical integration. The initial condition $z^0=2.0$, $v_z^0=0.2$, and the parameter $v=10$ are the same for all the four cases, but the parameter d is different, i.e., $d=8.7$, 9.4, 11.3, and 51, respectively.

The existence of the four regions can be explained as follows. The equation of motion in the z direction is

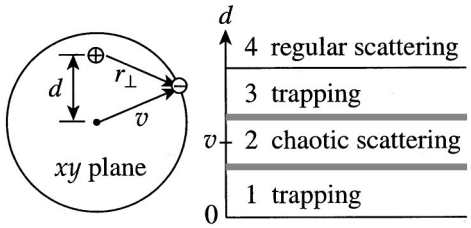

FIG. 10. Four different regions of motion.

$$\ddot{z}=-\frac{z}{(z^2+r_\perp^2)^{3/2}}, \tag{22}$$

where $r_\perp$ is the component of $\boldsymbol{r}$ perpendicular to the z direction. If $d\ll v$, then $r_\perp\approx v$, and Eq. (22) may be approximated as

$$\ddot{z}\approx-\frac{z}{(z^2+v^2)^{3/2}}. \tag{23}$$

On the other hand, if $d\gg v$, then $r_\perp\approx d$, and Eq. (22) may be approximated as

$$\ddot{z}\approx-\frac{z}{(z^2+d^2)^{3/2}}. \tag{24}$$

In each of the above two cases, we see a well-defined potential in the z direction from the equation of motion. If the total energy (i.e., the potential energy plus the kinetic energy) in the z direction is negative, the electron is trapped. Then for a proper initial condition such that the total energy is negative in each case, we have two trapping regions, denoted by region 1 and region 3 in Fig. 10.

For each potential if we increase the energy to the positive region, then we obtain the scattering motion. The interaction for the potential (23) is relatively larger than the potential (24). As a result, the chaotic scattering region is much larger in region 2 than in the region around the border between 3 and 4. Indeed, there exists a chaotic scattering region between 3 and 4. However, this region is so narrow that one cannot easily detect the chaotic scattering.

VI. FRACTAL STRUCTURE

It is well known that whenever we have a chaotic motion, there appears a fractal structure in some variables. In this section we show the fractal structure in the v_z^f, i.e., the value of v_z when the electron escapes to infinity, and the bouncing number n_z of the electron, where n_z is defined as the number of times v_z changes its sign before the electron escapes.

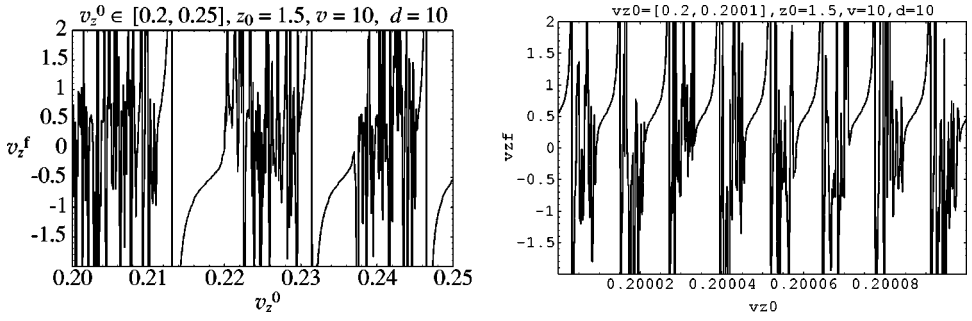

FIG. 11. Fractal structure obtained from the map in v_z^f vs v_z^0 for initial conditions $v_z^0\in$ (a) [0.2,0.25] and (b) [0.2,0.2001] $z^0=1.5$, $v=10$, and $d=10$.

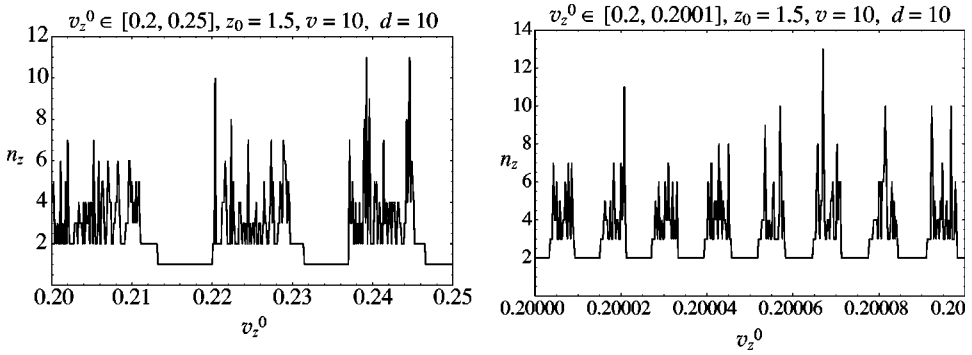

FIG. 12. Fractal structure obtained from the map in n_z vs v_z^0 for initial conditions $v_z^0 \in$ (a) [0.2,0.25] and (b) [0.2,0.2001], $z^0 = 1.5$, $v = 10$, and $d = 10$.

In Fig. 11(a), we show v_z^f as a function of v_z^0, with $v_z^0 \in [0.2,0.25]$, $z^0 = 1.5$, $v = 10$, and $d = 10$. It is seen that by slightly changing $V_z^0 = 0$, there are regions where v_z^f has a big change. This indicates the sensitivity in the initial condition. Moreover, there are smooth regions where v_z^f changes slowly. This shows that even inside the chaotic scattering regime, there exist regular regions.

In Fig. 11(b), we magnify a small section in v_z^0, i.e., $v_z^0 \in [0.2,0.2001]$ to see the fractal structure. This figure shows that inside the chaotic scattering regime, there is self similarity, which is typical of the fractal structure.

In Fig. 12(a), we show n_z vs v_z^0 for the same domain of Fig. 11(a). It can be seen that whenever n_z is constant, v_z^f is smooth, while in the chaotic region for v_z^f, we have the chaotic region for n_z. We again magnify the same interval in v_z^0 for n_z, as shown in Fig. 12(b), and one can see again the fractal structure in n_z.

VII. WIDTH OF CHAOTIC SCATTERING REGION

In this section, we estimate the size of the chaotic scattering region. For the case that v is small, the effect of the Coulomb force becomes a large perturbation over the cyclotron motion. This suggest that the smaller the velocity, the wider the chaotic region. In this section, we shall verify this prediction and numerically estimate the width of the chaotic region in the impact parameter as a function of v. However, our map is restricted only for the large values of v. For this reason, we perform the numerical integration of the equation of motion to find the width, instead of using our map.

We take the initial condition of the electron to be parallel to z with a velocity v. In this case, the initial condition is specified by the impact-parameter b and the velocity v, and we use the numerical integration to compute the width δb of the chaotic region for fixed v. Since the chaotic scattering region is much lager in region 2 in Fig. 10, we restrict our interest in this domain.

In order to compute δb, we need to define the upper bound and the lower bound of the chaotic region. To this end we first note that if b is too large, there is no bouncing motion of the electron, i.e., $n_z = 0$. For this case we have a regular scattering. Hence, the upper bound of the chaotic motion is determined by the boundary in b between $n_z = 0$ and $n_z \neq 0$. On the other hand, if b is too small, there is only one bouncing, i.e., $n_z = 1$, which corresponds to the other regular scattering. Hence, the lower bound of the chaotic motion is determined by the boundary in b for small b region between $n_z = 1$ and $n_z \neq 1$.

In Fig. 13, we show δb as a function of v from the results of the numerical integration. We see that v decreases as δb increases. The chaotic scattering is more likely to be observed for small v.

VIII. CONCLUDING REMARKS

For the case $v \gg 1$, we have derived a magneto-Coulomb map which has produced a good agreement with the numerical integration of the equation of motion. Using our map, we could predict a long-time behavior of the electron scattering in the chaotic regime. We have found that there appear four different regions of the motion by changing the distance d of the guiding center line of the cyclotron motion of the electron from the ion. Our map has shown that the fractal structure in the final velocity v_z^f and in the bouncing number n_z. We have also shown that the width of the chaotic scattering region becomes larger for smaller velocity v.

Suppose this scattering occurs in the plasma environment, then one can expect that plasma transport may become anomalous under the influence of the chaotic scattering. Our results suggest that the smaller v, the more anomalous the plasma transport. In the following we present several plasma environments, where $v \lesssim 1$. These cases are the ultracold neutral plasma [11], the white dwarf atmosphere, the neutron star atmosphere, with $v = 1.0$, 2.4, and 0.5, respectively. We expect the chaotic scattering has a stronger influence on these plasma environments. With the relation $\frac{3}{2} k_B T_e = \frac{1}{2} m_e (v \omega_c r_0)^2$, where T_e is the electron temperature, the dimensionless velocity can be expressed as

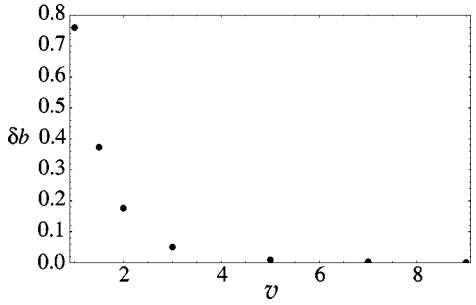

FIG. 13. Width δb of chaotic scattering region in the impact-parameter b as a function of initial velocity v.

TABLE I. Representative plasmas where chaotic scattering is predicted.

Plasma environments	Ultracold neutral plasma	White dwarf atmosphere	Neutron star atmosphere
T_e (K)	0.1	5.0×10^{4}	1.0×10^{6}
B (T)	4.0×10^{-4}	1.0×10^{4}	1.0×10^{8}
v	1.0	2.4	0.5
n_e (m^{-3})	2.0×10^{15}	1.0×10^{22}	1.0×10^{30}
$n_e^{-1/3}$ (m)	7.9×10^{-6}	4.6×10^{-8}	1.0×10^{-10}
r_0 (m)	3.7×10^{-5}	4.3×10^{-10}	9.2×10^{-13}
δb (m)	2.8×10^{-5}	1.0×10^{-9}	1.3×10^{-12}
b_{90} (m)	5.6×10^{-5}	1.1×10^{-10}	5.6×10^{-12}
ρ_e (m)	3.0×10^{-5}	8.6×10^{-10}	3.8×10^{-13}
λ_{De} (m)	4.9×10^{-7}	1.5×10^{-7}	6.9×10^{-11}
λ_e (m)	2.4×10^{-7}	3.3×10^{-10}	7.5×10^{-11}

$$v=(3k_B)^{1/2}(4\pi\epsilon_0 m_e^2)^{1/3}e^{-1}\frac{T_e^{1/2}}{(ZB)^{1/3}}$$

$$=[0.18\ \ \mathrm{K}^{-1/2}\,\mathrm{T}^{1/3}]\frac{T_e^{1/2}}{(ZB)^{1/3}}, \tag{25}$$

where and K and T denote Kelvin and Tesla. Table I lists some relative parameters for these three plasma environments. The parameters b_{90}, λ_e and λ_{De} are the impact parameter for 90° Rutherford scattering, thermal DeBroglie wavelength and Debye length in the dimensional units, respectively,

$$b_{90}=\frac{Ze^2}{12\pi\epsilon_0 k_B T_e}, \tag{26}$$

$$\lambda_e=\frac{2\pi\hbar}{\sqrt{2\pi m_e k_B T_e}}, \tag{27}$$

$$\lambda_{De}=\sqrt{\frac{\epsilon_0 k_B T_e}{n_e e^2}}. \tag{28}$$

Finally we give a comment on the effect of the radiation dumping. During the cyclotron motion, the electron loses energy because of the radiation. In this paper, we have neglected this effect. Here we estimate the radiation energy loss and show that the loss is very small. Let us consider the dimensionless power $P(t)$ radiated by an electron undergoing a dimensionless acceleration $a(t)$. It is given by

$$P(t)=\frac{\omega_c}{m_e}\frac{e^2}{6\pi\epsilon_0 c^3}a^2(t)$$

$$=\frac{e^3}{6\pi\epsilon_0 c^3 m_e^2}Ba^2(t)$$

$$=[1.1\times10^{-12}\ \ \mathrm{T}^{-1}]B\,a^2(t), \tag{29}$$

and the radiated energy is

$$\delta\mathcal{E}=\int dt\,P(t)=[1.1\times10^{-12}\ \ \mathrm{T}^{-1}]B\int dt\,a^2(t). \tag{30}$$

In the case of $v\sim1$, we have $a(t)\sim1$. Then the incident electron has an energy $\mathcal{E}=\frac{1}{2}v^2\sim1$. We can see from Eq. (30) that, in a time period of thousands cyclotron periods or less the energy radiated from an electron can be neglected, compared to the electron energy $\mathcal{E}$.

For the case where many ions are distributed randomly in space, one can apply our map for each ion and introduce the multimagneto-Coulomb map. This corresponds to the Lorentz model in statistical physics. We hope to estimate the transport coefficients in this multi-magneto-Coulomb map elsewhere.

ACKNOWLEDGMENTS

The authors thank Professor I. Prigogine and R. Balescu for helpful suggestions and interesting discussions. This work was supported by the Engineering Research Program of the Office of Basic Energy Science at the U.S. Department of Energy through Grant Nos. DE-FG03-96ER54346 and DE-FG03-94ER14465, the NSF-ATM9907637, the Robert A. Welch Foundation through Grant No. F-0365, the European Commission through Project No. HPHA-CT-2001-40002, the National Lottery of Belgium, and the Comminauté Française de Belgique.

[1] J.B. Delos, S.K. Knudson, and D.W. Noid, Phys. Rev. A **30**, 1208 (1984).
[2] G. Schmidt, E.E. Kunhardt, and J.L. Godino, Phys. Rev. E **62**, 7512 (2000).
[3] R. Gajewski, Physica (Utrecht) **47**, 975 (1970).
[4] J.B. Delos, S.K. Knudson, and D.W. Noid, Phys. Rev. A **28**, 7 (1983).
[5] H. Hasegawa, M. Robnik, and G. Wunner, Prog. Theor. Phys. Suppl. **98**, 198 (1989).
[6] B. Hu, W. Horton, C. Chiu, and T. Petrosky, Phys. Plasmas **9**, 1116 (2002).
[7] H. Friedrich and D. Wintgen, Phys. Rep. **183**, 37 (1989).
[8] M. Robnik, J. Phys. A **14**, 3195 (1981).
[9] C. L. Siegel and J. K. Moser, *Lectures on Celestial Mechanics* (Springer-Verlag, Berlin 1971).
[10] T. Petrosky, Phys. Lett. A **117**, 328 (1986).
[11] T.C. Killian, S. Kulin, S.D. Bergeson, L.A. Orozco, C. Orzel, and S.L. Rolston, Phys. Rev. Lett. **83**, 4776 (1999).